

Millefeuille-like Cellular Structures of Biopolymer Blend Foams Prepared by the Foam Injection Molding Technique

*Dongho Kim, Yuta Hikima, Masahiro Ohshima**

Dept of Chemical Engineering, Kyoto University, Kyoto, 615–8510, Japan

E-mail: ohshima.masahiro.2w@kyoto-u.ac.jp

Abstract: Microcellular foams with unique cellular structures were prepared from poly(lactic acid) (PLA) and poly(butylene succinate-co-adipate) (PBSA) blends using a foam injection molding technique with a core-back operation. PLA and PBSA are biopolymers that are partially miscible with each other. When these biopolymers were blended, several blend morphologies appeared that were found to be dependent on the blend ratio. The blend morphologies and thermal and rheological properties of polymer blends with PLA/PBSA ratios of 100/0, 30/70, 50/50, 70/30, and 0/100 were observed, and the cellular structures of their foams were investigated. While most of the polymer blends showed sea and island structures, a polymer blend with a PLA/PBSA ratio of 50/50 showed a layered structure for the two polymers in which the continuous phases of both polymers were elongated along the flow direction used for injection molding. By utilizing the unique blend morphology and the difference in the viscosities of the two polymers, a millefeuille-like microcellular structure was created from a 50/50 blend. Foams with millefeuille-like cellular structures show unique anisotropic mechanical properties, and this study reveals a method for preparing foams of this type.

1. Introduction

In the past three decades, biodegradable polyesters have been actively studied as substitutes for petroleum-based polymers. ^[1-4] Poly(lactic acid) (PLA) is an aliphatic polyester that can be produced from several bioresources, such as corn and sugarcane. PLA has been investigated from many perspectives, including processing characteristics such as extrusion, injection molding and foaming. ^[5] Because of its biodegradability, biocompatibility, and high stiffness and strength, PLA has been widely used in packaging or biomedical applications. ^[6-8] However, despite these advantages, the application of PLA has been limited due to several weaknesses, such as brittleness, low melt strength, slow crystallization rate, narrow processing windows and material cost. Many attempts have been made to overcome these weaknesses and improve processability, even for polymer foaming processes. For example, the degree of crystallinity and the mechanical, rheological and gas barrier properties of PLA have been modified by manipulating the ratio of L- and D-lactic acid stereoisomers. ^[9] Rheological and thermal properties have been controlled by several methods, such as the addition of a branched chain structure with a chain extender ^[10-12], a change in molecular weight ^[13] and the addition of nanoclay ^[14-16] or cellulose fiber. ^[17]

Polymer blending was also investigated as another scheme for modifying the properties and foamability of PLA. PLA is often blended with other flexible and biodegradable polymers, such as poly(butylene succinate) (PBS)^[18-28] and poly(butylene succinate-co-adipate) (PBSA)^[30-38]. The thermal properties, rheologies, and morphologies of PLA and PBSA blends have been characterized by several researchers. Lascano et al.^[30] reported that when blending PLA with PBSA, the tensile moduli of PLA/PBSA blends decreased and the elongation-at-break was enhanced with increasing amounts of PBSA component. Consequently, the brittleness of PLA was restrained, and the ductility was improved. Lee

et al.^[31] and Wang et al.^[32] observed the morphologies for PLA/PBSA blends with various blend ratios. For a PLA ratio above 60 wt.%, PBSA existed as droplet-shaped dispersed domains in the PLA matrix. However, when the PLA ratio was less than 40 wt.%, PLA existed as droplet-shaped domains in the PBSA matrix. They also reported that phase inversion occurred at a PLA to PBSA ratio of approximately 50/50. Eslami et al. ^[33,34] investigated the rheological properties of PLA, PBSA, and their blends and concluded that when blending PLA with PBSA, weak strain-hardening behavior appeared at a low strain rate; the melt strength of PLA was improved with increasing PBSA content.

Compared with the research carried out with PLA/PBS blend foams ^[24-28], there are few investigations of PLA/PBSA blend foams. Pradeep et al.^[37] used PBSA as a second polymer and conducted foam injection molding with CO₂ to examine the effect of PBSA on blend foamability. Their experimental results showed that the crystallinities and storage moduli of foams were improved by controlling the compatibility of the two polymers. Using blends composed of 75 wt.% PLA and 25 wt.% PBSA, Nofar et al. examined the effects of the PBSA dispersed domain on crystallization behaviors, rheological properties, morphologies and foamability of their blended beads. ^[40] Past studies for both PLA/PBS and PLA/PBSA foams have focused on foamability; either PBS or PBSA showed a droplet-shaped dispersed domain, indicating that the dispersed domain played a role as a bubble nucleating agent. ^[25, 27, 38, 40] Our previous studies have also established that a dispersed domain can be used as a bubble nucleating agent and that the bubble nucleation site can be changed from the domains themselves to the interface between two polymers; this depends on the solubility of the physical blowing agent in the polymers, the viscosity differences between domain and matrix, as well as the interfacial tension between polymers. ^[39-41]

In this study, we investigated the relationship between blend morphology and the cell structures of PLA/PBSA foams. Our primary interest was to investigate the foamability of the blends and the resulting cell structure of PLA/PBSA, especially for blends with 50/50 blend ratios, in which both polymers show co-continuous domains. As far as the authors are aware, no attention has been given to foaming any polymer blend with a co-continuous morphology. After measuring basic properties, such as the crystallization temperature, melting temperature, and viscosity, for polymer blends with PLA to PBSA blend ratios of 100/0, 30/70, 50/50, 70/30, and 0/100, foam injection molding experiments were conducted using nitrogen (N₂) as a blowing agent.

Blend morphology is drastically changed by the compatibility of blended polymers and also by the processing conditions. Injection molding can produce a blend morphology highly oriented along a flow direction. Using the oriented blend morphology, a polymer foam with a unique cellular structure was produced. The effects of blend morphology, thermal properties, and viscosity on the cellular structure and the mechanical properties of the resulting foams were investigated.

2. Material Preparation and Foam Injection Molding

2.1 Materials

The polymers used in this study are commercially available: PLA, (4032D, Nature Works, USA) and PBSA (FD92PB, PTT MCC Biochem, Thai). PLA is semicrystalline with an L-lactide content of ca. 98.6 wt.%, and its melt flow rate (MFR) is 7 g/min at 210 °C with a 2.16 kg weight. The MFR of PBSA is 4 g/min at 190 °C with a 2.16 kg weight.

Both polymers were used as received. The physical blowing agent used for foam-injection molding was nitrogen (N_2) with 99.7% purity (Izumi-Sangyo Corp., Japan).

2.2 Foaming Experiments

The experiments were carried out using a 35-tonnage clamping force foam injection molding (FIM) MuCell® machine (J35EL III-F, Japan Steel Works, Japan) with a gas dosing system (SII TRJ-10-A-MPD Trexel Inc., Showa Gas Products, Japan). A cylindrical screw 20 mm in diameter with an L/D ratio of 24:1 and a mold with a rectangular cavity (70 mm × 50 mm × 1 mm) were used for injection molding. A single phase of molten polymer and 0.1 wt.% N_2 was injected into the mold cavity. Then, to foam the polymers, a part of the mold was quickly opened in one direction after a certain dwelling (holding) time, which is called core-back operation or precise mold-opening operation. This operation notably enlarges the cavity volume, rapidly reduces the polymer pressure in the cavity and simultaneously initiates bubble nucleation. The details of the mold geometry and the operation of FIM were described in our previous papers [42-46].

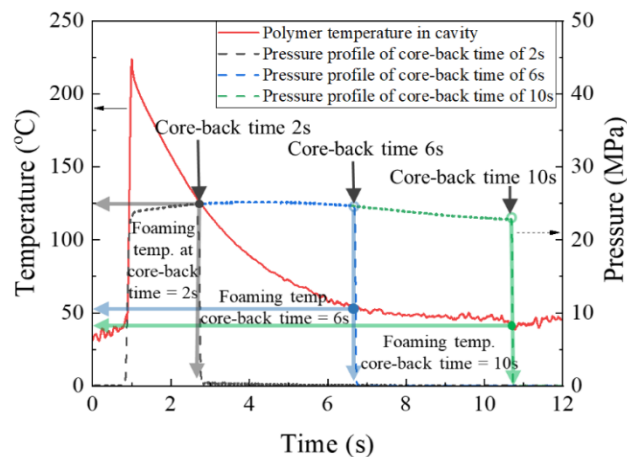


Figure 1. Temperature and pressure profiles for the polymer injected into the mold cavity during one injection cycle time.

Two infrared temperature sensors and two pressure sensors were independently deployed in the rectangular mold cavity to measure polymer temperatures and pressures at different locations in the cavity: one location was close to the inlet, and the other was at the flow end, as shown in the supporting information (**Figure S1**). By averaging the temperatures and pressures at two points of three injection cycles, the temperature and pressure profiles during a cycle of injection molding were calculated and plotted against the processing time, as shown in **Figure 1**. The profiles were recorded by using a data acquisition device (Mold Marshaling system EPD-001, Futaba, Japan). Infrared temperature sensors were used to measure the polymer temperature at a point approximately 0.4 mm inside from the mold-polymer interface in the thickness direction. Because the thickness of the polymer in the cavity before foaming was 1 mm, the measured temperatures were considered to be similar to those at the center of the polymer in the thickness direction. As shown in Figure 1, the temperature exponentially decreased while the pressure increased and remained constant during the holding (dwelling) operation. When the core-back operation was conducted at the end of the holding operation, the pressure of the polymer drastically decreased to atmospheric pressure. The core-back timing, i.e., at which point the part of the mold was opened, is equivalent to the end of the holding operation. The core-back time was defined by the time elapsed from the start of polymer injection to the onset of core-back operation. The cooling rate of the polymer in the holding process was estimated from the recorded temperature profiles. It was found to be in the range -40 to -8 °C/s. The cooling rate affected the crystallization behavior of the polymers.

The temperature at the core-back time, which was noted as the foaming temperature, was calculated from the temperature and pressure profiles. As illustrated in Figure 1, the

temperature of the polymer in the cavity decreased after the polymer was injected into the mold cavity. By delaying the core-back timing, i.e., making the core-back time longer, the foaming temperature was lowered. In other words, the foaming temperature can be changed by manipulating the core-back time.

In this study, blends with blend ratios of 100/0, 70/30, 50/50, 30/70, and 0/100 were prepared by dry-blending PLA with PBSA pellets in the hopper of an injection molding machine. Foam-injection molding was conducted for each polymer blend using N₂ as the physical blowing agent. The core-back time was changed within the range 1 second to 12 seconds to observe the effects of the foaming temperature on the cell structure and the width of the operation windows. Other processing parameters are summarized in **Table 1**. At least 10 injection moldings were performed at each core-back time to confirm reproducibility.

Table 1. Operating conditions for the solid/foam injection molding process.

Processing condition for solid/foam injection molding		
Barrel Temperature	[°C]	7 zones from tip of barrel to hopper
PLA/PBSA		210, 210, 210, 210, 210, 160, 120
PLA alone		210, 210, 210, 210, 210, 210, 180
Mold Temperature	[°C]	40
Dwelling Pressure	[MPa]	40
Injection Velocity	[mm/s]	120
Initial Thickness of Cavity	[mm]	1
Core-back Rate	[mm/s]	20
Core-back Distance	[mm]	2
Expansion Ratio		3
Core-back Timing	[s]	1–12

2.3 Thermal Properties

The thermal properties of the polymers were measured using conventional differential scanning calorimetry (DSC) (7020, Hitachi Ltd., Japan) and fast-scanning chip calorimetry (FSC, Mettler-Toledo Flash DSC1, Mettler-Toledo, LLC, USA). For the conventional DSC measurements, specimens were prepared by cutting nonfoamed (solid) injection-molded polymers into small pieces with a weight of approximately 5–6 mg. The measurements were conducted under N₂ purging. To obtain the first cooling curve, the temperature was raised to 200 °C, held for 3 min, and then cooled to -60 °C at a 10 °C/min cooling rate. To obtain the 2nd heating curves, the temperature was held at a lower temperature of -60 °C for 20 min and heated to 200 °C at 10 °C/min. The measurement was repeated at least twice. From the 2nd heating curves, the crystallinity of PLA, χ_c , was calculated using Equation (1),

$$\chi_c (\%) = \frac{\Delta H_m - \Delta H_{cc}}{\Delta H_f X_{PLA}} \times 100 \quad (1)$$

where ΔH_m , ΔH_{cc} and X_{PLA} are the enthalpy of melting, the enthalpy of cold crystallization and the weight fraction of PLA in the polymer blend, respectively. ΔH_f is the enthalpy of fusion defined by the enthalpy of melting per gram for 100% crystalline PLA, which is equal to 93.6 J/g. [33]

FSC measurements were also conducted under a N₂ purge to simulate the rapid cooling condition for injection molding. Specimens 10–20 μm in thickness and 50–100 μm in width and length were prepared by cutting the injection-molded polymers with a microtome (MRS-F, Nihon Koki Seisakusho Ltd, Japan). For measurements of nonisothermal crystallization, the specimens were heated to 200 °C first, held for 1 s, and then cooled to -90 °C by changing the cooling rate within the range -1 °C/s to -1000 °C/s. For the case in which the crystallization peak could not be observed in the rapid cooling

process, the presence of crystals was confirmed from the heating curve obtained by a discrete method, which involved heating at 1000 °C/s immediately after rapid cooling at rates of -10 °C/s, -15 °C/s, and -20 °C/s. Both DSC and FSC measurements were repeated using an injection molded blend and neat polymers.

2.4 Rheological properties

To observe the effects of blend morphology on rheological properties, disk-shaped specimens 25 mm in diameter and 2 mm in thickness were prepared from injection-molded polymers as well as from polymers blended by a mixer (Labo-Plastomill, Toyoseiki, Japan). The preparation conditions for injection-molded polymers are given in Table 1. The mixer-blended polymer was prepared by mixing the polymer at 200 °C at 10 rpm for the first 3 minutes and then at 50 rpm for the subsequent 4 minutes. Disk-shaped specimens were prepared by cutting the polymer products into small pieces and then hot-pressing at 200 °C under a mechanical pressure of 20 MPa for 10 min. A dynamic frequency sweep test was carried out using a rotational rheometer (ARES, TA Instruments Inc., USA) operated at 210 °C with 1% strain in the frequency range 0.1 rad/s to 100 rad/s. The temperature sweep test was also conducted at a frequency of 1 rad/s with two different shear strains, 1% and 10%. In the tests, the temperature was reduced from 200 °C to room temperature with a cooling rate of -2 °C/min. To observe the rheological behaviors of PLA and PBSA in the low-temperature region, torsion tests were conducted at 1% strain in the temperature range 30 °C to 100 °C. All rheological measurements were repeated at least three times for each blend and for neat polymers.

2.5 Characterization of Morphology and Cell Structure

Blend morphologies were observed by scanning electron microscopy (SEM) (JSM-6700F, JEOL Ltd., Japan). The specimens were prepared by cutting the injection-molded polymers into small pieces. To eliminate the shear effect on the blend morphology of the specimen, annealed specimens were prepared by placing the injection molded polymer into a small rectangular shaped mold on a hot-press machine and holding the polymer at 200 °C under a mechanical pressure of 10 MPa for 10 min. Then, the specimens were immersed in liquid N₂ for 10 min and fractured to observe the cross-sectional area by SEM. Prior to the SEM observation, the fractured surface was coated with gold using an ion coater (VPS-020 Quick coater, Ulvac Kiko Ltd., Japan) for 1 min. The cell structures of foams were observed using another SEM system (Tiny-SEM Mighty-8, Technex, Japan) after cryogenic treatment of the foam injection-molded polymers.

2.6 ATR-FTIR spectroscopy and FTIR spectroscopic imaging

Attenuated total reflection-Fourier transform infrared spectroscopy (ATR-FTIR) measurements were conducted for PLA/PBSA blends to confirm the blend morphology. A diamond ATR accessory (Goldengate, Specac Inc. UK) was used with the FTIR instrument (Spectrum 100, PerkinElmer Inc. USA). ATR-FTIR spectra were acquired in the wavenumber range 5500 cm⁻¹ to 700 cm⁻¹ with a resolution of 4 cm⁻¹. The accumulation number was set to 10. To evaluate the chemical morphologies of the PLA/PBSA blends, an FTIR spectroscopy imaging system (Spotlight 400, PerkinElmer Inc. USA) was also used. For FTIR imaging measurements, specimens were prepared by slicing the nonfoamed (solid) injection-molded polymers into thin sheets of

approximately 10–30 μm in thickness. FTIR images were acquired in transmission mode in the wavenumber range between 5500 and 750 cm^{-1} with a resolution of 4 cm^{-1} . The number of scans per pixel was set to 16 for measurements of specimens and 120 for the background measurement. The pixel size of the FTIR image was 6.25 μm x 6.25 μm .

2.7 Mechanical properties

Compression tests were conducted in two schemes to investigate the anisotropic mechanical properties of PLA, PBSA and their blended foams using a universal testing machine (Autograph, AGS-J, Shimadzu, Japan). The machine was equipped with a 1000 N load cell. Because some foams had many elongated cells and PLA/PBSA (50/50) showed a layered structure oriented along the flow direction, compression tests were conducted by applying the stress to two different foam axes (core-back direction and injection direction). To apply the stress to the foams in the direction parallel to the core-back direction (expansion direction), the specimen was prepared by keeping the skin layers and cutting out the middle part of the foam into a piece with a width and length of 10 mm and 3 mm, respectively. Then, the specimen was placed onto the machine table so that the skin layers could be aligned perpendicular to the direction of the applied stress (Scheme 1). To apply stress to the foams parallel to the flow direction (injection direction), specimens with widths, lengths and thicknesses of 10 mm, 3 mm, and 5 mm, respectively, were placed onto the machine table so that the skin layers were aligned parallel to the direction of the applied stress (Scheme 2). After setting the crosshead speed to 10 mm/min, both schemes for the compression tests were performed until the compressive force reached 1000 N to obtain a stress-strain (S-S) curve. The compressive strength was

determined by the stress value at a strain of 20%, and the compressive modulus was calculated from the slope at which the stress increased rapidly.

3. Results and Discussion

3.1 Thermal Properties

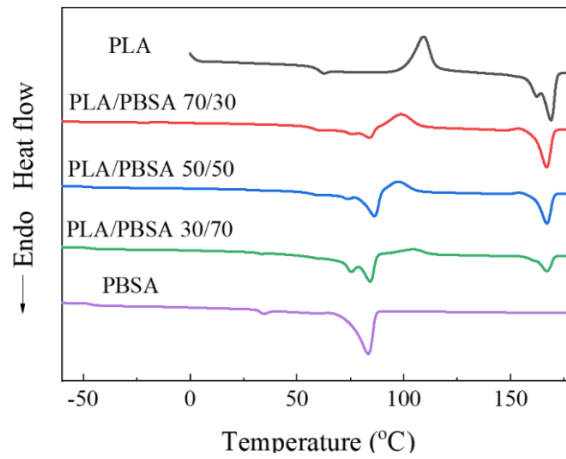


Figure 2. DSC second heating curves for PLA, PBSA and their blends.

Table 2. Thermal properties of injection molded polymers.

PBSA contents	T_g		T_{cc}	T_m				ΔH_{cc}	ΔH_m	χ_c
	PBSA	PLA	PLA	PBSA		PLA		PLA	PLA	PLA
				T_{m1}	T_{m2}	T_{m1}	T_{m2}			
wt%	°C	°C	°C	°C	°C	°C	°C	J/g	J/g	%
0	-	62.9	109.2	-	-	162.3	168.7	30.3	33.5	3.4
30	-48.0	60.4	100.5	75.6	83.7	-	166.8	15.6	26.5	16.6
50	-49.2	59.4	101.5	73.4	85.4	-	166.8	11.5	18.4	14.6
70	-48.3	58.7	99.3	75.2	84.1	-	166.9	6.6	10.9	15.0
100	-48.8	-	-	83.3	-	-	-	-	-	-

Figure 2 shows the DSC heating curves measured for PLA, PBSA, and PLA/PBSA blends in the second cycle. All thermal properties obtained from the heating curves are summarized in Table 2. The glass transition temperatures, T_g , for PLA and PBSA were observed individually in the heat curves obtained for the PLA/PBSA blends. The T_g of PBSA was slightly increased in the presence of PLA, while the T_g of PLA was slightly decreased to lower temperatures with increasing PBSA content. This is an indication of the partial miscibility of the two polymers. The blended polymers showed three melting peaks: one is associated with PLA crystals, and the others are bimodal peaks associated with PBSA.

The double melting peak observed for the PLA/PBSA blend has already been reported by Lee et al. [24] Double peaks for the melting point, T_m , of neat PLA appeared at 162.3 °C and 168.7 °C and were converted to a single peak with increasing PBSA content. The cold crystallization temperature, T_{cc} , for neat PLA was approximately 109 °C. As the PBSA content was increased, T_{cc} decreased to 99 °C. The decrease in T_{cc} is explained by the plasticization effect of PBSA, which enhanced the chain mobility of PLA. [33] Interestingly, the crystallinity of neat PLA crystallized with a cooling rate of -10 °C was approximately 3.4%. When blended with PBSA, the crystallinity increased dramatically to 14.6–16.6%, which indicates enhancement of PLA crystallization by PBSA.

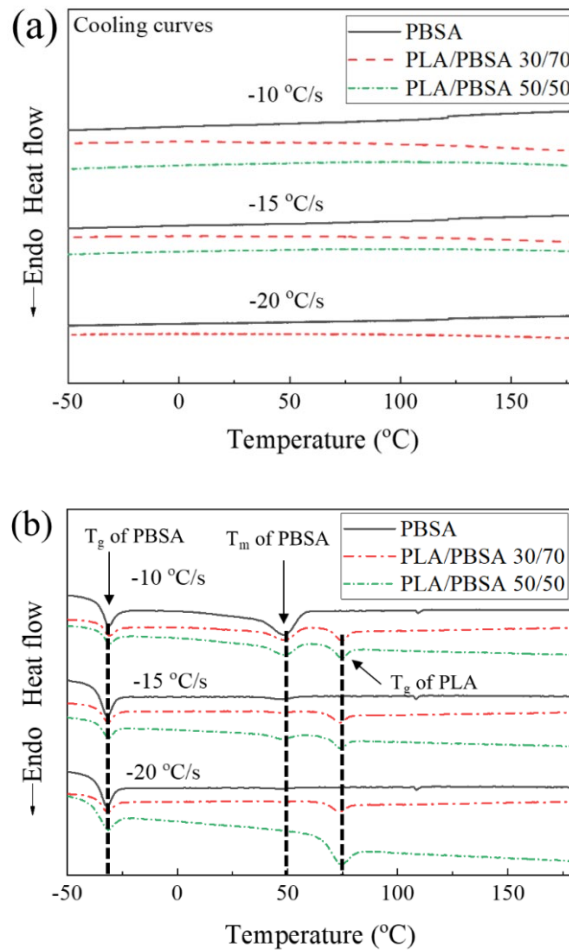


Figure 3. Cooling and heating curves for polymers treated at various rapid cooling rates: (a) cooling curves; (b) heating curves obtained by heating at 1000 °C/s after cooling at -10 °C/s, -15 °C/s and -20 °C/s.

Figures 3(a) and **(b)** show the FSC curves obtained for PBSA and PLA/PBSA blends with blend ratios of 30/70 and 50/50. The cooling curves obtained for cooling rates of -10 °C/s, -15 °C/s, and -20 °C/s are shown in Figure 3(a), and those produced during the heating stage after rapid cooling are shown in Figure 3(b). The heating rate was set to 1000 °C/s to prevent cold crystallization during the heating process. Unlike conventional DSC, FSC can cool or heat the polymer at very high rates and allow thermal property measurements under conditions similar to those of practical foam injection molding. The

heat absorption associated with crystallization was difficult to observe at any cooling rate and any blend ratio, as shown in Figure 3(a). However, as shown in Figure 3(b), the FSC heating curves indicated that the T_m for PBSA was approximately 40–50 °C for all heating curves obtained after cooling at rates of -10 °C/s and -15 °C/s, but T_m was not observed for the specimen heated after cooling at a rate of -20 °C/s. PBSA crystallized at cooling rates slower than -15 °C/s. On the other hand, the T_m for PLA was not observed for specimens cooled at any rate. However, strain-induced crystallization of PLA may occur in the injection molding process. The presence of strain-induced PLA crystals can increase the viscosities of blends to a value larger than those shown in Figure 5.

3.2 Rheological properties

Figure 4 shows the results obtained from the frequency sweep tests. Figure 4(a) shows the storage moduli, G' , for PLA, PBSA, and their blends. G' gradually decreased with decreasing frequency and increasing PLA content. The descending rate for G' as a function of frequency became milder for PLA/PBSA (50/50) in the low-frequency region. Because PLA/PBSA (50/50) showed a co-continuous two-phase morphology, it is possible that the PLA and PBSA phases penetrated each other and formed a network morphology. The presence of such a network could lead to a milder descending rate, as mentioned by Hernández-Alamilla et al. They report that a plateau region for G' appeared in the low-frequency region when a network structure was established in polymers [46].

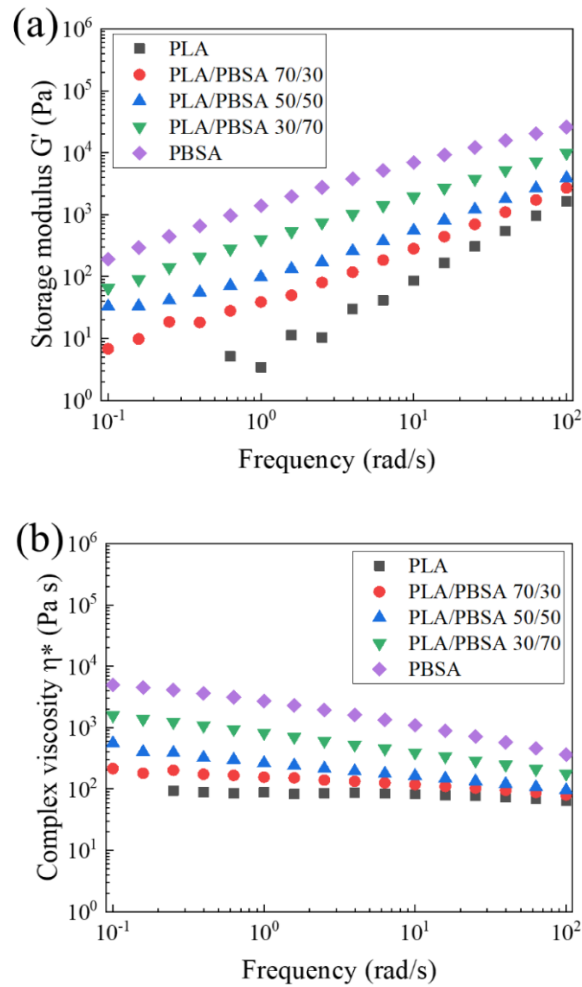


Figure 4. Frequency dependence of (a) G' and (b) η^* for PLA, PBSA and their blends (210 °C, strain 1%).

Figure 4(b) shows the complex viscosity, η^* . η^* for PLA showed Newtonian fluid behavior at low shear frequencies and shear-thinning behavior at high frequencies. η^* for neat PBSA showed shear thinning behavior at all measured frequencies. Lee et al. ^[24] and Eslami et al. ^[26] reported similar observations for their PBSA. The deviation from Newtonian fluid behavior for neat PLA at low frequency became larger as the PBSA

content in the blended polymers was increased. The increase in viscosity with the decreasing frequency suppressed bubble growth and kept the bubble size small.

Figure 5 shows the results for temperature sweep tests performed for PLA, PBSA and their blends. η^* for PBSA shows a high value compared to PLA and their blends, even at high temperatures, and it also shows a slow increase in viscosity even when the temperature was decreased. However, PLA showed the lowest η^* at high temperature, but η^* rapidly increased as the temperature decreased. Therefore, the sensitivity of η^* in blends as a function of temperature was increased by increasing the PLA content.

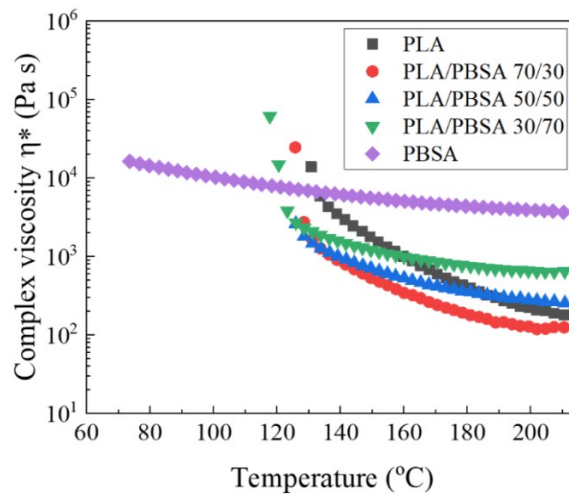
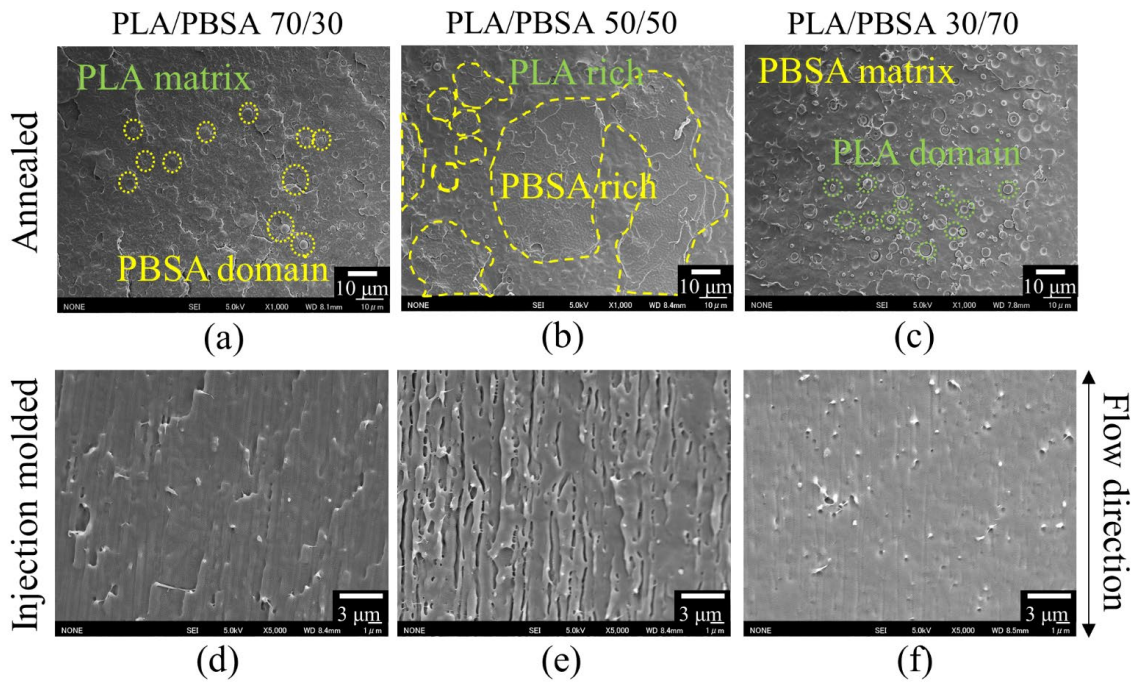


Figure 5. Temperature dependence of η^* for PLA, PSBA and their blends (frequency 1 rad/s, strain 1%, cooled at -2 °C/min).

3.3 Morphologies of polymer blends

Figure 6 shows SEM images of blend morphologies for both annealed and injection-molded PLA/PBSA. As shown in Figure 6(a)-(c), the samples annealed on a hot press after injection molding showed clear morphologies. When the PBSA content was low, a sea and island morphology appeared in which PBSA formed droplet-shaped minor domains (Figure 6(a)). For a PBSA to PLA ratio of 50/50, the samples showed a co-continuous two-phase morphology (Figure 6(b)). When the PBSA content was increased above 50 wt.%, PLA formed droplet-shaped minor domains (Figure 6(c)).



It was difficult to identify the blend morphology for polymer samples prepared by injection molding without annealing. The sea and island morphologies were not observed clearly for PLA/PBSA (70/30) and (30/70). However, every domain was likely elongated along the flow direction. As shown in Figure 6(e), PLA/PBSA (50/50) appeared to show a two-phase co-continuous morphology in which the two phases showed different surface roughness: one domain was smooth and the other was rough, which may correspond to the PLA and PBSA phases. The morphology observed in Figure 6(e) might be due to artifacts. Thus, the two-phase, co-continuous morphology of PLA/PBSA (50/50) was confirmed by using another method, i.e., FTIR.

3.4 IR spectra and chemical imaging

Figure 7(a) shows ATR-FTIR spectra for PLA/PBSA blends with various blend ratios. The absorbance of the spectral band at 870 cm^{-1} increased as the PLA content was increased, while the absorbance at 920 cm^{-1} increased as the PBSA content was increased. Therefore, assuming that the spectral bands at 870 cm^{-1} and 920 cm^{-1} indicate the PLA and PBSA contents, respectively, FTIR spectroscopic imaging was performed to visualize the chemical (PLA and PBSA) distribution in nonfoamed injection-molded PLA/PBSA blends. **Figure 7(b)** shows FTIR images for the absorbance ratios of spectral bands at 870 cm^{-1} to those at 920 cm^{-1} for a cross-sectional area of the PLA/PBSA blends. In the FTIR chemical images, the red color represents PLA, and dark blue represents PBSA-rich regions. The vertical direction for the images denotes the sample thickness, and the horizontal direction denotes the direction of polymer flow (MD) induced by injection molding. The upper and lower edge of each map correspond to surfaces of the injection-

molded samples. The colors at the upper and bottom regions tend to be yellow and red, which indicates that the region near the surface is PLA-rich. This can be considered a viscosity encapsulation phenomenon: at a high injection temperature, i.e., 210 °C, and a high shear rate, the PLA viscosity was lower than that of PBSA, as shown in Figure 5. Flow occurred through a sprue of the mold used in the injection molding process. Therefore, for PLA/PBSA, which has a significant difference in viscosities for the blend constituents in the molten state, PLA shifted toward the wall of the sprue due to its lower viscosity.

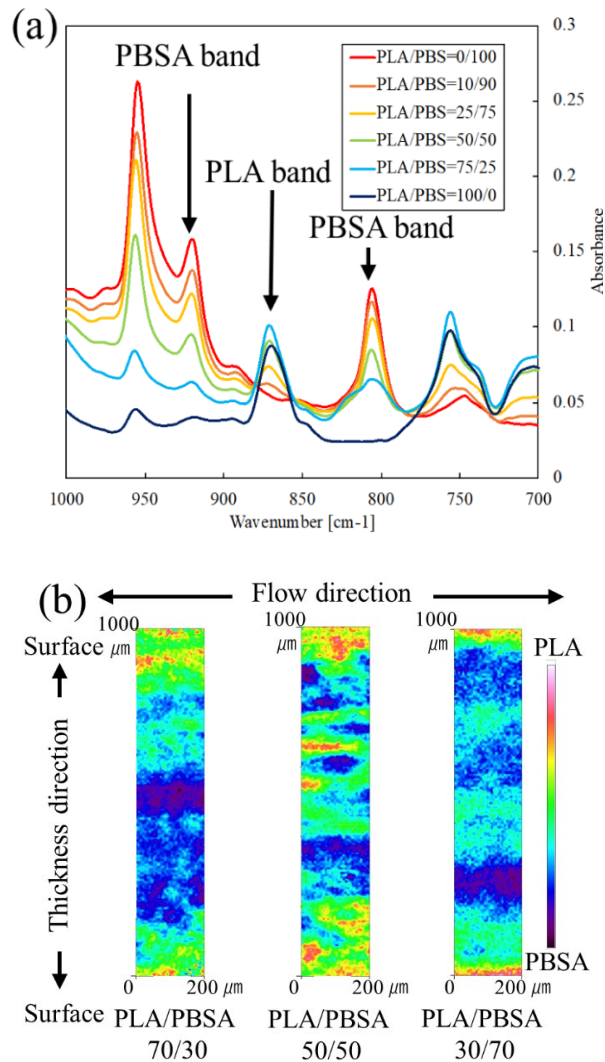
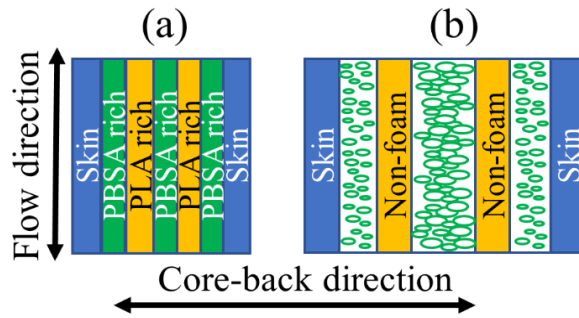


Figure 7. IR spectrum and chemical imaging results: (a) ATR-FTIR spectra and (b) FTIR images of the absorbance ratios for 870 cm^{-1} (PLA) and 920 cm^{-1} (PBSA) bands of the nonfoamed PLA/PBSA blends.

In PLA/PBSA (50/50), a PLA-rich layer and PBSA-rich layer alternately appeared and formed a multilayered structure. The FTIR images show that the PLA and PBSA phases were elongated and highly oriented along the flow direction.

3.5 Cellular Structures of Foams



Our previous study investigated the potential of using dispersed domains as bubble nucleating sites in blended polymers and found that when the domains had a higher solubility and diffusivity for the physical blowing agent and a lower viscosity than the matrix polymer, bubble nucleation was selectively enhanced in the dispersed domain. [40-42] As shown in Figures 6 and 7, the PLA/PBSA blend with a blend ratio of 50:50 was partially miscible, and a highly oriented blend morphology was formed by injection

molding. Thus, bubble nucleation was enhanced at the highly elongated PBSA phase, as illustrated in **Figure 8**.

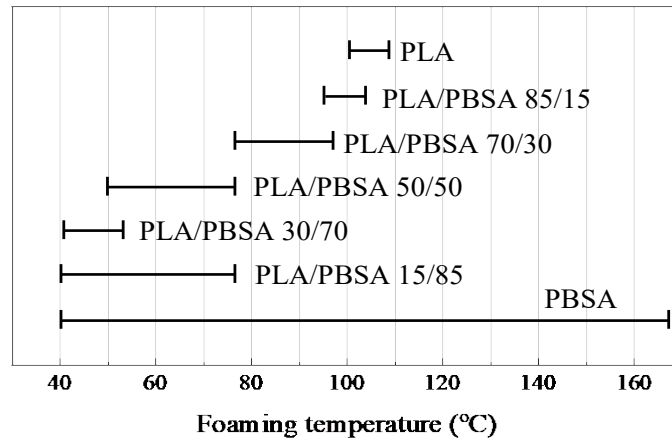


Figure 9. Temperature windows for preparing microcellular foams with expansion ratios of 3.

In foam injection molding with core-back operations, the core-back timing can be manipulated as explained in the previous section. The temperature of the polymer in the cavity decreased toward 40 °C (the mold temperature) after the polymer was injected into the cavity. The temperature of the polymer at the onset of the core-back operation was defined as the foaming temperature. For each blend and neat polymer, the core-back time was manipulated within the range 1 to 12 seconds to intentionally change the foaming temperature. By observing the expansion ratio and the cellular structure of the resulting foams, the windows for foaming temperatures were determined.

Figure 9 shows the foaming temperature windows used for preparing microcellular foams with an expansion ratio of 3 for each polymer. The upper limit for the window was determined as the highest foaming temperature at which the polymer could be foamed without having a balloon-like hollow structure or large cells in its foam. The lower limit

of the window was the lowest foaming temperature at which polymer could be foamed by achieving an expansion ratio of 3. The lowest foaming temperature limit for the PBSA-rich polymer blend and PBSA alone was 40 °C, which was determined by the mold temperature itself. Namely, the foaming temperature could not be made lower than the mold temperature by changing any other operation parameters.

As shown in Figure 9, neat PBSA was foamed over a wide range of foaming temperatures, while PLA exhibited the narrowest range. The change in viscosity for PBSA in the temperature range 180 °C to 60 °C was not large compared with that of PLA, as shown in Figure 5. The wide foaming temperature window of PBSA can be associated with the temperature sensitivity of PBSA viscosity. The foaming temperature window for PLA was narrower than that we reported in the past. ^[44] This is because the mold temperature was reduced from 60 to 40 °C. For the blends, the window was narrower, and its upper limit moved to a lower temperature in the presence of PLA. This is due to a decrease in viscosity with increasing PLA content. As illustrated in Figure 5, the viscosities for the PLA/PBSA blends and neat PLA showed values lower than that for PBSA in the temperature range 120 °C to 210 °C. The lower the viscosity, the more likely it was that large bubbles would form in the foam. The upper limit for the foaming temperature window was lowered to prevent the formation of such large bubbles when blending PLA. When PLA became the major component in the blend morphology, the window was narrowed, and the lower limit for the foaming window was moved to a higher temperature. As shown in Figure 5, as more PLA was blended, the viscosities of the blends became higher than that of PBSA at temperatures lower than 120 °C. Higher viscosities increased the likelihood that the expansion ratio could not reach the desired level. Furthermore, Figure 5 shows that as the PLA content was increased, the slope for

increasing viscosity with decreasing temperature became steeper. The temperature dependence of the viscosity strongly affected the width of the foaming temperature window.

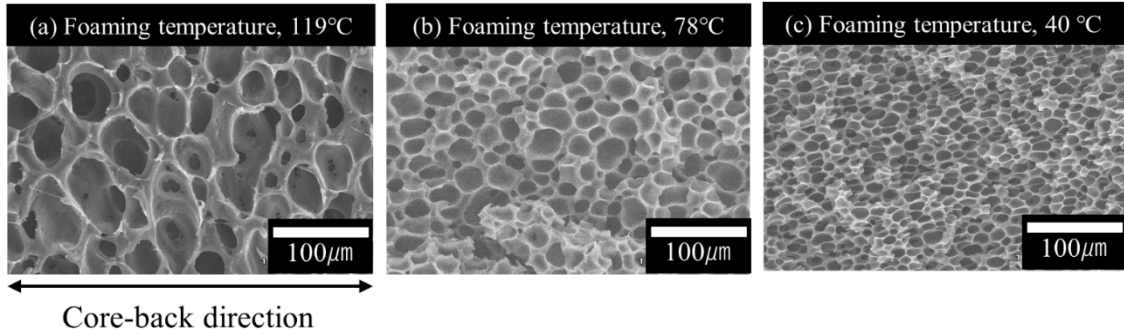
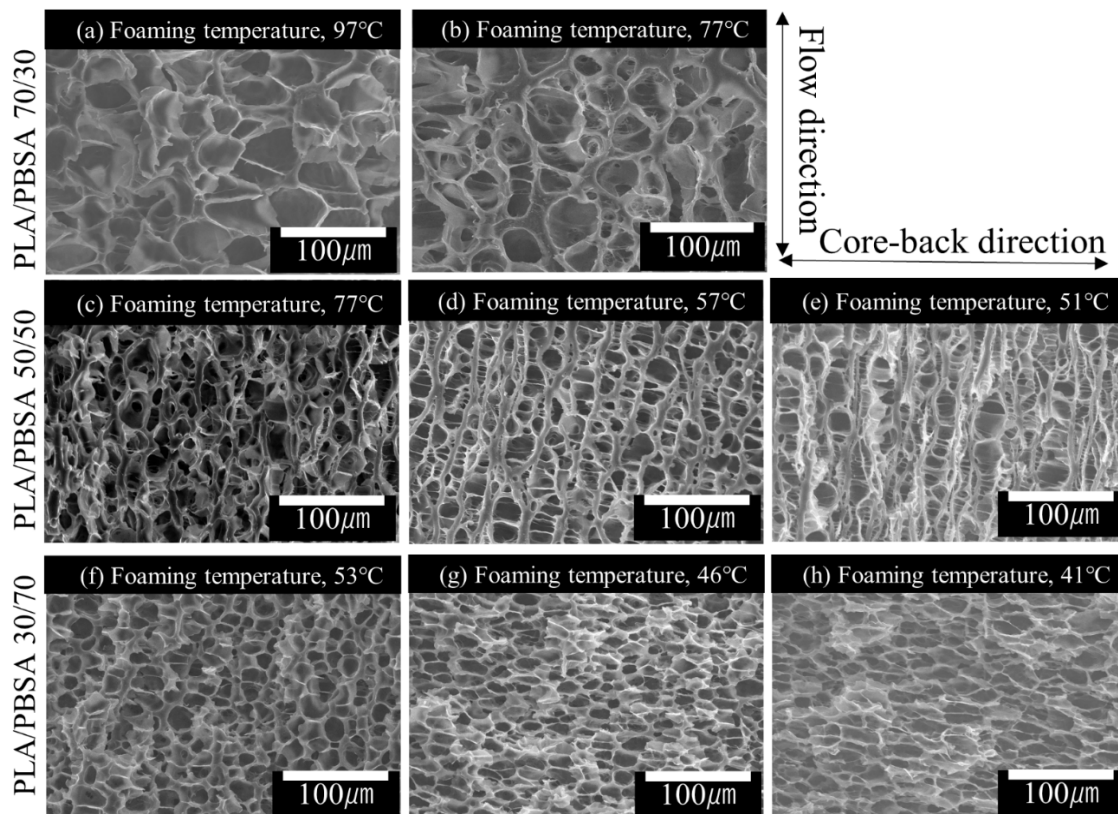


Figure 10. SEM images of cellular structures of foams comprising PBSA alone with an expansion ratio of 3 prepared at different foaming temperatures.

Figures 10 and **11** show SEM images for the cross-sectional areas of PBSA and PLA/PBSA (70/30), (50/50), and (30/70) foams, respectively. Foams with an expansion ratio of 3 were prepared in the abovementioned foaming window by manipulating the core-back timing. All SEM images were taken with a view parallel to the core-back direction. The foaming temperature is indicated in the upper right corner of each image. In Figures 10 and 11, the horizontal direction corresponds to the direction of the foamed sample thickness or the core-back direction, and the vertical direction corresponds to the flow direction (MD).

As shown in Figure 5, the cellular structure of neat PBSA foam was uniform, and cells were well packed at any foaming temperature. At low foaming temperatures, the cell size was small, but it became larger with increasing foaming temperature.



In general, the cell size was increased by increasing the foaming temperature. However, the cell structure of PLA/PBSA (70/30) foams tended to be more uniform and showed structures similar to a hexagonal close-packed structure. The cell size was unchanged even when the foaming temperature was increased. As shown in Figure 9, PLA was easily foamed at higher temperatures, but it was difficult to foam PLA at lower temperatures. In the PLA/PBSA (70/30) foams, the PLA matrix did not foam well at low foaming temperatures. Upon increasing the foaming temperature, more cells nucleated in the PLA matrix, and then the cells became more uniform.

The PLA/PBSA (30/70) foam showed cells smaller than those of other foams. This is because the PLA domains acted as bubble nucleating agents and increased the number of bubbles. As a result, the cell size was reduced. By reducing the foaming temperature to 41 °C, the cell size of PLA/PBSA (30/70) foams was slightly increased, and at the same time, the cell was elongated in the core-back direction, as shown in Figure 11(h). Figure S3 contains lower magnification SEM images of the cross-sectional area of PLA/PBSA (30/70) foams. It is clear that the degree of elongation of the cells increased with decreasing foaming temperature. In particular, the degree of elongation was higher for cells located around the center of foams prepared with low foaming temperatures. The injected polymer was cooled in the mold cavity from interfaces with the mold, and a temperature gradient was established in the polymer along the thickness direction (i.e., core-back direction). As the dwelling (core-back) time was increased, the foaming temperature decreased and the temperature gradient increased. Consequently, the skin layer became thicker, and the foamable area became narrower. To keep the expansion ratio at three despite the narrowed foamable area, the cells around the center should be elongated more than the cells located near the interface with the mold.

The cellular structure of PLA/PBSA (50/50) foamed at a temperature higher than 77 °C (Figure 11(a)) showed a uniform cell structure similar to that of PBSA foamed at 119 °C. However, as the foaming temperature was decreased, the cells tended to align along the flow direction and eventually form a Millefeuille-like structure. The order of the alignment increased as the foaming temperature was decreased, as illustrated in Figure 11(b) and (c). The injection molding process created a layered blend morphology oriented along the flow direction, as shown in Figure 7. Due to the layered morphology and the effect of temperature on viscosity, a millefeuille-like cellular structure was created.

As shown in Figure 5, the viscosity of PLA increased with decreases in the foaming temperature below 120 °C, while that for PBSA did not increase drastically and remained at approximately 10^4 Pa s within the temperature range 80 °C to 160 °C. The results from torsion tests also showed that the complex viscosity of neat PLA was high at 10^9 Pa s, while that for PSBA was 10^8 Pa s in the temperature range 40 °C to 60 °C, as shown in **Figure S2** of the supporting information. Figures 5 and S2 show that the difference in viscosity between PLA and PBSA became larger at temperatures in the range 40 °C to 80 °C. If strain-induced crystallization occurred in the PLA phase, the difference in viscosities for PLA and PBSA would be further enlarged. With higher viscosity, the foamability of the PLA domain would decrease. In the PLA/PBSA blends, the effect of temperature on the viscosities of both the PLA and PBSA phases was expected to be the same. Namely, by tuning the foaming temperature, one could foam the PBSA phase while keeping the PLA phase unfoamed. When the foaming temperature was far below 100 °C, the unfoamed PLA phase was aligned along the flow direction, but the PBSA phase could be foamed, as shown in Figures 9 and 10.

3.6 Mechanical properties

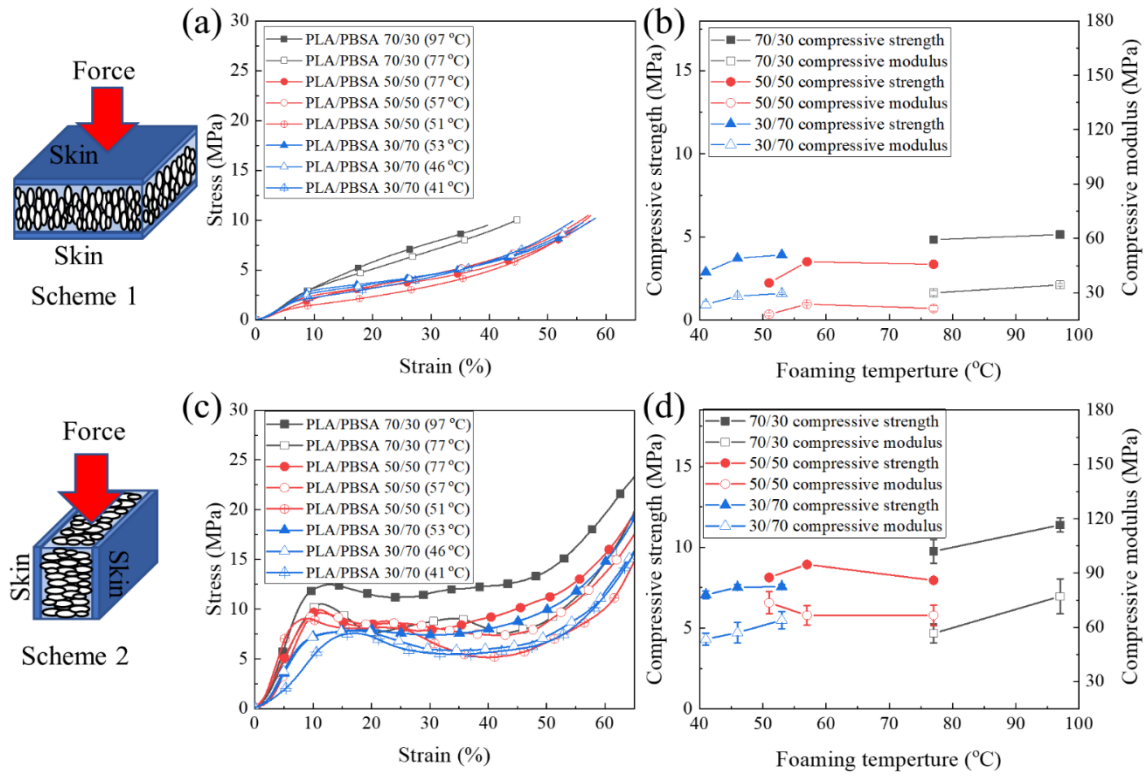


Figure 12. Results of compression tests. (a, b) Measured by Scheme 1 and (c, d) measured by Scheme 2, (a, c) S-S curves, (b, d) compressive strengths and moduli.

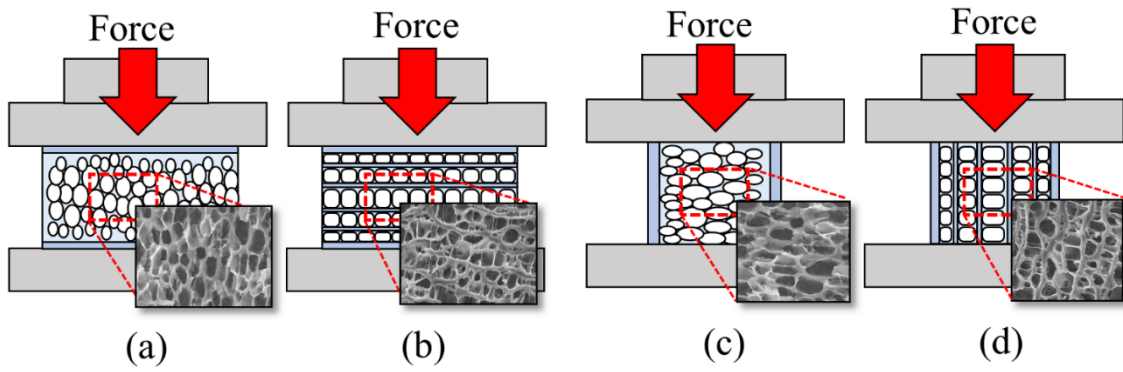


Figure 12 shows the results of the compression tests. Figure 12(a) shows the strain-stress (S-S) curves obtained by applying stress to a specimen parallel to the core-back (expansion) direction (Scheme 1), where the skin layers are located in the direction perpendicular to the applied force, as illustrated in Figures 13(a) and (b). Figure 12(c) shows the S-S curves obtained by applying stress to the specimen parallel to the injection direction (Scheme 2); skin layers are located in a direction parallel to that of the applied force, as illustrated in Figures 13(c) and (d). The compressive strengths and moduli were determined from the resulting S-S curves, and the results are illustrated in Figures 12(b) and (d).

Figures 12(b) and (d) show some interesting results: i) the compressive strengths and moduli increased as the foaming temperature was increased for all polymer samples except PLA/PBSA (50/50); ii) PLA/PBSA (50/50) foams possessed strong anisotropic mechanical properties. The compressive strength and modulus of PLA/PBSA (50/50) do not show monotonous increases with increasing foaming temperature. In the Scheme 2 test, the compressive modulus of PLA/PBSA (50/50) foamed at a low temperature (51 °C) was as high as that for PLA/PBSA (70/30), as indicated by the red open circle.

As shown in Figure 11, the PLA/PBSA (70/30) foam showed a hexagonally packed cell structure at higher foaming temperatures. Ali, N. B. et al. showed that the hexagonal packing structure exhibited the strongest mechanical properties. ^[47] It is thought that the hexagonally packed cell structure of PLA/PBSA (70/30) foam provided a higher compressive modulus and strength at high foaming temperatures.

PLA/PBSA (30/70) also showed an increase in compressive strength and modulus with increasing foaming temperature. For the blend foamed at a low foaming temperature, the

presence of elongated cells decreased the compressive strength and modulus. PLA/PBSA (50/50) foamed at low temperature (51 °C) showed anisotropic mechanical properties: the lowest mechanical properties were observed in the Scheme 1 test, but a high modulus was observed in Scheme 2. These anisotropic mechanical properties were produced by the multilayered cell structure, for which nonfoamed PLA was layered in the flow direction and the cells were aligned between the nonfoamed PLA layers. The presence of multiple layers of nonfoamed PLA led to a high compressive modulus for stresses applied in the direction parallel to the layers. On the other hand, the thickness of the cell walls between PLA layers became thinner as the foaming temperature was lowered. The cell structure resulted in a low compressive strength and modulus as a function of the stress applied in the direction perpendicular to the layers.

4. Conclusion

In this study, PLA/PBSA blends with different blend ratios were foamed by a core-back foam injection molding process. In previous studies, PBSA has been used to enhance the foamability of PLA; however, in this study, PLA/PBSA blends were investigated with several blend ratios. The thermal properties and viscosities of PLA/PBSA blends were measured. With these data, this study focused on the potential of using the layered, highly oriented co-continuous two-phase morphology of a PLA/PBSA (50/50) blend as a controlling factor for creating a unique cell structure. A millefeuille-like cellular structure was created for PLA/PBSA (50/50). We investigated the mechanism for formation of the unique cellular foam morphology from the perspectives of rheological properties, crystallization behavior, and phase morphology of both components in the blends. It was

speculated that the interesting cell structure was created by synergistic effects among three factors, i.e., differences in viscosities of the two components in the blend, blend morphology, and processing (foaming) conditions.

This study shows that the millefeuille-like cellular structure provides a unique anisotropic mechanical property. This layered cell structure has the potential to provide other anisotropic properties, such as gas permeability or heat conductivity.

References

- [1] M. Okada, Chemical syntheses of biodegradable polymers, *Prog. Polym. Sci.* **27** **2002**, 87-133
- [2] D. Garlotta, A Literature Review of Poly (Lactic Acid), *J. Polym. Environ.* **2001**, *9*, 63–84.
- [3] J.R. Dorgan, H. Lehermeier, M. Mang, Thermal and Rheological Properties of Commercial-Grade Poly(Lactic Acid)s, *Journal of Polym. Environ.* **2000**, *8*, 1–9
- [4] D.W. Grijpma, A.J Pennings, (Co)polymers of L-lactide, Mechanical properties, *Macromol. Chem. Phys.* **1994**, *195*, 1649- I663
- [5] M. Nofar, C.B. Park, Polylactide Foams: Fundamentals, Manufacturing, and Application, PDL Handbook Series, Elsevier, **2017**, 1-272, ISBN 9780128139912
- [6] R. Auras, B. Harte, S. Selke, An Overview of Polylactides as Packaging Materials, *Macromol. Biosci.* **2004**, *4*, 835–864.

- [7] F.J. Hua, G.E. Kim, J. D. Lee, Y. K. Son, D. S. Lee, Macroporous Poly (L-Lactide) Scaffold 1. Preparation of a Macroporous Scaffold by Liquid-Liquid Phase Separation of a PLLA-Dioxane-Water System, *J. Biomed. Mater. Res.* **2002**, 63, 2, 161-167
- [8] M S. Lope, A.L. Jardini, R.M. Filho, Poly (Lactic Acid) Production for Tissue Engineering Applications, *Procedia Eng.* **2012**, 42, 1402-1413
- [9] H. Urayama, S.L. Moon, Y. Kimura, Microstructure and thermal properties of polylactides with different L- and D-unit sequences; *Macromol Mater Eng.* **2003**, 288, 137-143
- [10] S. Pilla, A. Kramschuster, L. Yang, S. Gong, L.S. Turng, Microcellular injection-molding of polylactide with chain-extender', *Mater. Sci. Eng.* **2009**, C 29 1258-1265
- [11] Y. Corre, A. Maazouz, J. Duchet, J. Reignier, Batch foaming of chain extended PLA with supercritical CO₂: Influence of the rheological properties and the process parameters on the cellular structure, *J. of Supercritical Fluids* **2011**, 58 177-188
- [12] M. Mihai, M.A. Huneault, B. D. Favis, Rheology and Extrusion Foaming of Chain-Branched Poly(lactic acid), *Polym. Eng. Sci.* **2010**, 50, 3, 629-642
- [13] Y. Di, S. Iannace, E. Di Maio, L. Nicolais, Reactively Modified Poly(lactic acid): Properties and Foam Processing, *Macromol. Mater. Eng.* **2005**, 290 1083-1090.
- [14] A. Ameli, D. Jahani, M. Nofar, P. U. Jung, C. B. Park, Development of high void fraction polylactide composite foams using injection molding: Crystallization and Foaming Behavior', *Compost. Sci. Technol.* **2014**, 90, 88-95

- [15] A. Ameli, M. Nofar, D. Jahani, G. Rizvi, C.B. Park, Development of high void fraction polylactide composite foams using injection molding: Mechanical and thermal insulation properties, *Chem. Eng. J.* **2015**, 262, 78-87
- [16] Y. Di, S. Iannace, E. Di Maio, L. Nicolais, Poly(lactic acid) Organoclay Nanocomposites Thermal, Rheological Properties and Foam Processing, *J. Polym. Sci. B* **2005**, 43, 689–698
- [17] W. Ding, D. Jahani, E. Chang, A. Alemdar, C.B. Park, M. Sain, Development of PLA/cellulosic fiber composite foams using injection molding: Crystallization and foaming behaviors. *Compos. Part A, Appl. Sci. Manuf.* **2016**, 83, 130–139
- [18] A. Bhatia, R.K. Gupta, S.N. Bhattacharya, H.J. Choi, Compatibility of biodegradable poly (lactic acid) (PLA) and poly (butylene succinate) (PBS) blends for packaging application. *Korea Aust. Rheol. J.* **2007**, 19, 125–131.
- [19] L.Q. Xu, H.X. Huang, Relaxation Behavior of Poly(lactic acid)/Poly(butylene succinate) Blend and a New Method for Calculating Its Interfacial Tension. *J. Appl. Polym. Sci.* **2012**, 125, E272–E277.
- [20] Y. Deng, N.L. Thomas, Blending poly(butylene succinate) with poly(lactic acid): Ductility and phase inversion effects. *Eur. Polym. J.* **2015**, 71, 534–546
- [21] T. Yokohara, K. Okamoto, M. Yamaguchi,; Effect of the Shape of Dispersed Particles on the Thermal and Mechanical Properties of Biomass Polymer Blends Composed of Poly(L-lactide) and Poly(butylene succinate), *J. Appl. Polym. Sci.* **2010**, 117, 2226–2232
- [22] D. Wu, L. Yuan, E. Laredo, M. Zhang, W. Zhou, Interfacial properties,

- viscoelasticity, and thermal behaviors of poly(butylene succinate)/polylactide blend. *Ind. Eng. Chem. Res.* **2012**, *51*, 2290–2298
- [23] E. Hassan, Y. Wei, H. Jiao, Y. Muhuo, Dynamic mechanical properties and thermal stability of poly(lactic acid) and poly(butylene succinate) blends composites. *J. Fiber Bioeng. Informatics* **2013**, *6*, 85–94
- [24] P. Ma, X. Wang, B. Liu, Y. Li, S. Chen, Y. Zhang, G. Xu, Preparation and foaming extrusion behavior of polylactide acid/polybutylene succinate/montmorillonite nanocomposite. *J. Cell. Plast.* **2012**, *48*, 191–205
- [25] D. Aussawasathiena, K. Ketkulb, K. Hrimchuma, P. Threepopnatkulb, Effects of Poly(lactic acid) and Polybutylene Succinate Ratios on Properties of Composite Foams Containing Activated Carbons, AIP Conference Proceedings 2065, 030046, **2019**, doi.org/10.1063/1.5088304
- [26] P. Yu, H.Y. Mi, A. Huang, L.H. Geng, B.Y. Chen, T.R. Kuang, W.J. Mou, X.F. Peng, Effect of Poly(butylenes succinate) on Poly(lactic acid) Foaming Behavior: Formation of Open Cell Structure. *Ind. Eng. Chem. Res.* **2015**, *54*, 6199–6207
- [27] X. Shi, L. Wang, Y. Kang, J. Qin, J. Li, H. Zhang, X. Fan, Y. Liu, G. Zhang, Effect of poly(butylenes succinate) on the microcellular foaming of polylactide using supercritical carbon dioxide, *J. Polym. Res.* **2018**, *25*, 229, 1-12
- [28] J. Zhou, Z. Yao, C. Zhou, D. Wei, S. Li, Mechanical properties of PLA/PBS foamed composites reinforced by organophilic montmorillonite. *J. Appl. Polym. Sci.* **2014**, *131*, 9319–9326

- [29] Z. Lv, N. Zhao, Z. Wu, C. Zhu, Q. Li, Fabrication of Novel Open-Cell Foams of Poly(ϵ -caprolactone)/Poly(lactic acid) Blends for Tissue-Engineering Scaffolds. *Ind. Eng. Chem. Res.* **2018**, *57*, 12951–12958.
- [30] D. Lascano, L. Quiles-Carrillo, R. Balart, T. Boronat, N. Montanes, Toughened poly (lactic acid)-PLA formulations by binary blends with poly(butylene succinate-co-adipate)-PBSA and their shape memory behavior. *Materials (Basel)*. **2019**, *12*, doi:10.3390/ma12040622.
- [31] S. Lee, J.W. Lee, Characterization and processing of Biodegradable polymer blends of poly (lactic acid) with poly (butylene succinate adipate). *Korea-Australia Rheology Journal* **2005**, *17*, 2, 71–77
- [32] Y. Wang, J.F. Mano, Biodegradable Poly(L-lactic acid)/Poly(butylene succinate-co-adipate) Blends: Miscibility, Morphology, and Thermal Behavior. *J. Appl. Polym. Sci.* **2007**, *105*, 3204–3210
- [33] H. Eslami, M.R. Kamal, Effect of a chain extender on the rheological and mechanical properties of biodegradable poly(lactic acid)/poly[(butylene succinate)-co-adipate] blends. *J. Appl. Polym. Sci.* **2013**, *129*, 2418–2428
- [34] H. Eslami, M.R. Kamal, Elongational rheology of biodegradable poly(lactic acid)/poly[(butylene succinate)-co-adipate] binary blends and poly(lactic acid)/poly[(butylene succinate)-co-adipate]/clay ternary nanocomposites. *J. Appl. Polym. Sci.* **2013**, *127*, 2290–2306
- [35] V. Ojijo, S. Sinha Ray, R. Sadiku, Toughening of biodegradable polylactide/poly(butylene succinate- co -adipate) blends via in situ reactive

- compatibilization. *ACS Appl. Mater. Interfaces* **2013**, *5*, 4266–4276.
- [36] S.S. Ray, J. Bandyopadhyay, M. Bousmina, Thermal and thermomechanical properties of poly[(butylene succinate)-co-adipate] nanocomposite. *Polym. Degrad. Stab.* **2007**, *92*, 802–812
- [37] S. A. Pradeep, H. Kharbas, L. S. Turng, A. Avalos, J. G. Lawrence, S. Pilla, Investigation of Thermal and Thermomechanical Properties of Biodegradable PLA/PBSA Composites Processed via Supercritical Fluid-Assisted Foam Injection Molding, *Polymer* **2017**, *9*, 1, 22,1-18
- [38] M. Nofar, A. Tabatabaei, H. Sojoudiasli, C.B. Park, P.J. Carreau, M.C. Heuzey, M.R. Kamal, Mechanical and bead foaming behavior of PLA-PBAT and PLA-PBSA blends with different morphologies. *Eur. Polym. J.* **2017**, *90*, 231–244.
- [39] R. W. Sharudin, A. Nabil, K. Taki, M. Ohshima, Polypropylene-Dispersed Domain as Potential Nucleating Agent in PS and PMMA Solid-State Foaming, *J. Appl. Polym. Sci.* **2011**, *119*, 1042–1051
- [40] T. Nemoto, J. Takagi, M. Ohshima, Nanoscale Cellular Foams from a Poly(Propylene)-Rubber Blend, *Macromol. Mater. Eng.* **2008**, *293*, 12, 991-998,
- [41] T. Nemoto, J. Takagi, M. Ohshima, Nanocellular Foams-Cell Structure Difference Between Immiscible and Miscible PEEK/PEI Polymer Blends, *Polym. Eng. Sci.* **2010**, *50*, 12, 2408-2416
- [42] S. Ishihara, Y. Hikima, M. Ohshima, Preparation of Open Microcellular Polylactic Acid Foams with a Microfibrillar Additive using Coreback Foam Injection Molding Processes, *Cell. Plas.* **2018**, *54*, 4, 765-784

- [43] R. Miyamoto, S. Yasuhara, H. Shikuma, M. Ohshima, Preparation of Micro/Nanocellular Polypropylene Foam with Crystal Nucleating Agents, *Polym. Eng. Sci.* **2013**, 54, 9, 2075-2085
- [44] T. Ishikawa, K. Taki, M. Ohshima, Visual Observation and Numerical Studies of N₂ vs. CO₂ Foaming Behavior in Core-Back Foam Injection Molding. *Polym. Eng. Sci.* **2012**, 52, 4, 875-883
- [45] L. Wang, Y. Hikima, M. Ohshima, T. Sekiguchi, H. Yano, Evolution of cellular morphologies and crystalline structures in high-expansion isotactic polypropylene/cellulose nanofiber nanocomposite foams. *RSC Adv.* **2018**, 8, 15405–15416.
- [46] M. Hernández-Alamilla, A. Valadez-Gonzalez, The effect of two commercial melt strength enhancer additives on the thermal, rheological and morphological properties of polylactide, *J. Polym. Eng.* **2016**, 36(1): 31–41
- [47] N. B. Ali, M. Khlif, D. Hammami, C. Bradai, Mechanical and morphological characterization of spherical cell porous structures manufactured using FDM process. *Engineering Fracture Mechanics*, **2019**, 216, 106527

Supporting Information

Millefeuille-like Cellular Structure of Biopolymer Blend Foams by the Foam Injection Molding Technique

Dongho Kim^a, Yuta Hikima^a, Masahiro Ohshima^{a*}

^aDept of Chemical Engineering, Kyoto University, Kyoto 615-8510, Japan

*Corresponding author.

E-mail: ohshima.masahiro.2w@kyoto-u.ac.jp

1. Experimental procedures

1.1 Measurement of Temperature and Pressure of polymer in the mold cavity

The temperature and pressure of the polymer injected into the rectangular shaped cavity are measured by two infrared temperature sensors and two pressure sensors. The location of the sensors in the cavity is shown in **Figure S1**.

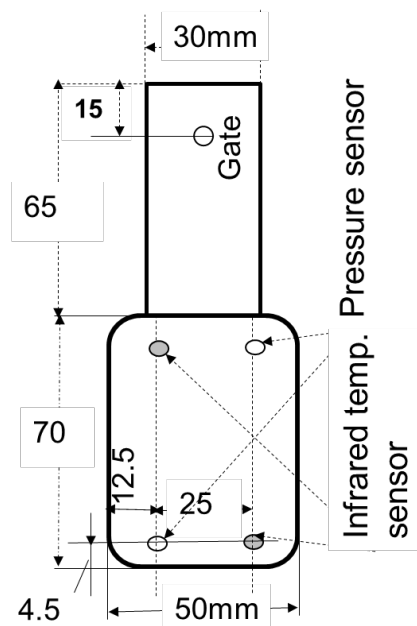


Figure S1. The geometry of the mold cavity and the locations of two temperature sensors and two pressure sensors.

1.2 Torsion test for measuring the rheological properties in low temperature range

The torsion test was conducted using a rotational rheometer (ARES, TA Instruments Inc., USA). The measurement was performed with the 1% strain at a frequency of 1 rad/s while increasing the temperature at the rate of 2 °C/min from 30 to 200 °C in a temperature sweep mode. The specimens, 10 mm in width, 30 mm in length, and 1 mm in thickness, were prepared by cutting the central part of the unfoamed injection-molded polymer products.

1.3 Three-point bending tests

The three-point bending tests were conducted using a universal testing machine (Autograph, AGS-J, Shimadzu, Japan). For the measurement, both hot-pressed film and foam injection molded polymers were used. As for the hot-pressed film, the unfoamed injection molded polymers of PLA, PBSA, and PLA/PBSA 50/50 were cut out into small pieces, placed in a mold with a thickness of 1 mm, and hot-pressed for 10 minutes with 20 MPa compression stress at 200°C. As for the foamed specimen, the foam injection-molded polymers of PLA, PBSA, and PLA/PBSA 50/50 were used. The rectangular-shaped specimen, 10 mm in width 30 mm in length, and 1 mm in thickness were prepared from the hot-pressed films and foam injection molded polymers at two different directions,

the machine direction (MD) and transverse direction (TD). The three-point bending tests were done at a crosshead speed of 5 mm/min with a force of 1000 N. The flexural strength σ_f and the flexural modulus E_f were calculated by Eqs (S1) and (S2), respectively.

$$\sigma_f = \frac{3FL}{2bd^2} \quad (\text{S1})$$

$$E_f = \frac{L^3m}{4bd^3} \quad (\text{S2})$$

where F and L are force and span. b and d represent respectively the width and the thickness of the specimen. m is the slope of the load vs deflection curve. By repeating the test five times for each specimen, the measurement values were averaged.

2. Results and discussion

2.1 Torsion test for measuring the rheological properties in low temperature range

Figure S2 shows the results of the torsion tests of PLA and PBSA. The complex viscosity η^* of PLA was 10^9 Pa s at 30 °C. With the increase of temperature, η^* started decreasing around 60 °C, which corresponded to the T_g of PLA, and then it increased around 90 °C, which corresponded to the cold crystallization of PLA. With the further increase of the temperature, PLA started melting around 160 °C, and the viscosity η^* decreased rapidly. In the case of PBSA, because the T_g of PBSA was -48.8 °C as shown in Table 2, the change in the viscosity η^* corresponding to the T_g was not observed in the

tested temperature range, and the viscosity η^* decreased at around its melting temperature, 80 °C.

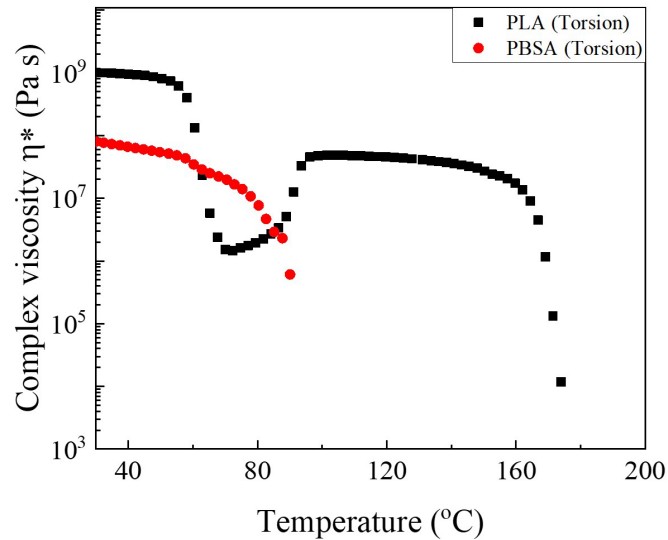


Figure S2. Temperature dependency of the absolute value of complex viscosity, η^* , of PLA and PBSA unfoamed samples measured by a torsion test (strain 1%, frequency 1 rad/s).

2.2 foam Microcellular structure

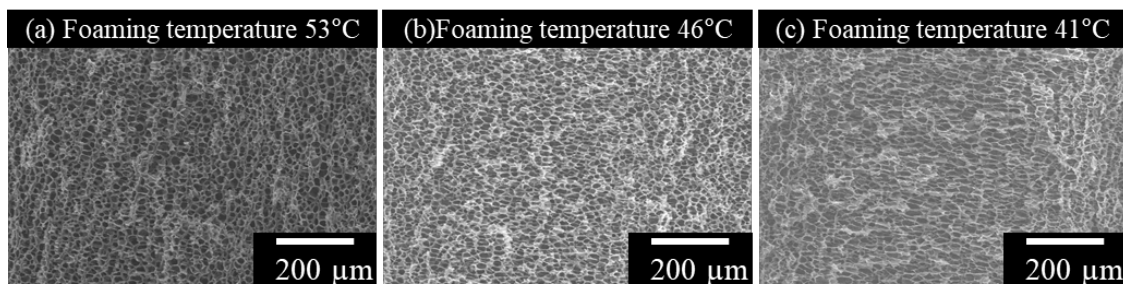


Figure S3. The low magnification SEM images of the cellular structure of the foams of PLA/PBSA 30/70 with the expansion ratio of 3 times prepared at different foaming temperatures.

2.3 Three-point bending test

Figure S4 shows the flexural strength and flexural modulus of PLA, PBSA, and PLA/PBSA 50/50 prepared from the hot-pressed films and the foams. The hot-pressed films (unfoamed) showed higher strength and modulus than the foamed specimens. Comparing the flexural strength and the modulus of the hot-pressed film of PLA with those of the hot-pressed films of polymer blend and PBSA, the flexural strength and the flexural modulus of PLA were quite high, those of PBSA were lowest and PLA/PBSA (50/50) blend was in the middle. A similar trend was observed in the results of foamed specimens. As for the dependency of polymer orientation on the flexural strength and modulus, the strength and the modulus of the specimen cut out along the flow direction (MD) shows a higher value than those of the specimen prepared along the transversal direction (TD).

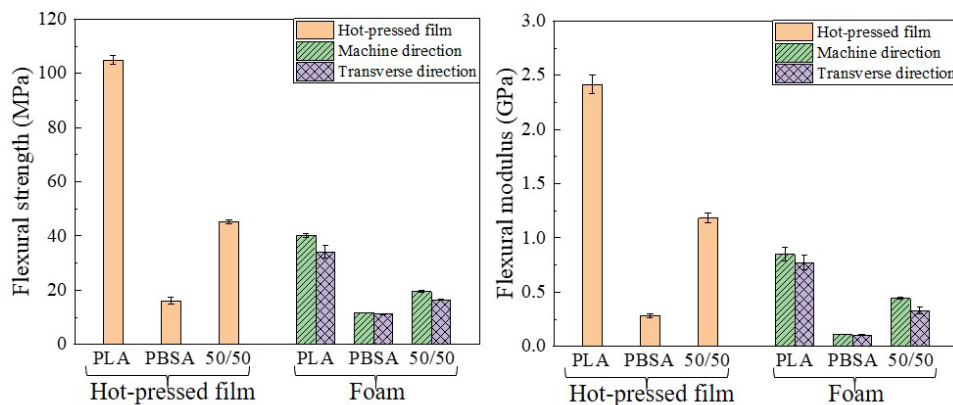


Figure S4 Results of three-point bending tests for PLA, PBSA, and PLA/PBSA 50/50 prepared from the hot-pressed films and the foams: (a) flexural strength, (b) flexural modulus.